ResearchGate

See discussions, stats, and author profiles for this publication at: https://www.researchgate.net/publication/49843765

Development and Applications of Fluorescent Indicators for Mg2+ and Zn2+

ARTICLE *in* THE JOURNAL OF PHYSICAL CHEMISTRY A · FEBRUARY 2011

Impact Factor: 2.69 · DOI: 10.1021/jp110305k · Source: PubMed

CITATIONS
83

READS
107

5 AUTHORS, INCLUDING:

Wenwu Qin
Lanzhou University
67 PUBLICATIONS **2,096** CITATIONS
SEE PROFILE

Wei Dou
Lanzhou University
83 PUBLICATIONS **1,330** CITATIONS
SEE PROFILE

Available from: Wenwu Qin
Retrieved on: 27 January 2016

THE JOURNAL OF PHYSICAL CHEMISTRY A

ARTICLE

pubs.acs.org/JPCA

Development and Applications of Fluorescent Indicators for Mg^{2+} and Zn^{2+}

Lina Wang, Wenwu Qin, Xiaoliang Tang, Wei Dou, and Weisheng Liu*

Key Laboratory of Nonferrous Metals Chemistry and Resources Utilization of Gansu Province and State Key Laboratory of Applied Organic Chemistry, College of Chemistry and Chemical Engineering, Lanzhou University, Lanzhou 730000, China

Supporting Information

ABSTRACT:

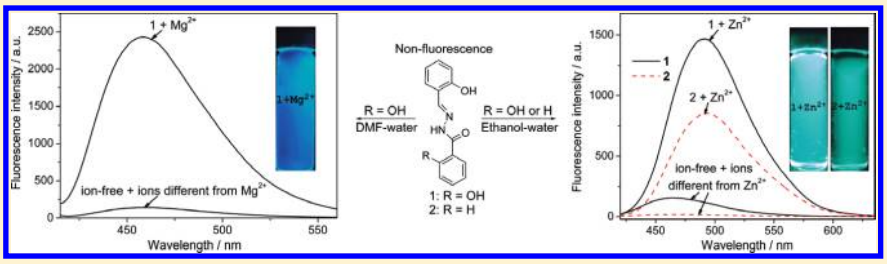

In a study of the spectroscopic behavior of two Schiff base derivatives, salicylaldehyde salicylhydrazone (**1**) and salicylaldehyde benzoylhydrazone (**2**), Schiff base **1** has high selectivity for Zn^{2+} ion not only in abiotic systems but also in living cells. The ion selectivity of **1** for Zn^{2+} can be switched for Mg^{2+} by swapping the solvent from ethanol−water to DMF (*N*,*N*-dimethylformamide)−water mixtures. Imine **2** is a good fluorescent probe for Zn^{2+} in ethanol−water media. Many other ions tested, such as Li^+, Na^+, Al^{3+}, K^+, Ca^{2+}, Cr^{3+}, Mn^{2+}, Fe^{3+}, Co^{2+}, Ni^{2+}, Cu^{2+}, Ag^+, Cd^{2+}, Sn^{2+}, Ba^{2+}, Hg^{2+}, and Pb^{2+}, failed to induce any spectral change in various solvents. The selectivity mechanism of **1** and **2** for metal ions is based on a combinational effect of proton transfer (ESPT), C═N isomerization, and chelation-enhanced fluorescence (CHEF). The coordination modes of the complexes were investigated.

INTRODUCTION

Fluorescent probes for metal ions have found widespread use not only in environmental monitoring but also in biological studies.[1] The development of highly sensitive fluorescent probes for metal ion analysis is an active research field.[2] Fluorescence offers significant advantages over other methods for metal ion detection and measurement because of its generally nondestructive character, high sensitivity, and instantaneous response.[3] Zinc and magnesium are indispensable for mediating many enzyme-catalyzed reactions in humans.[4] These elements play important roles in a wide variety of physiological and pathological processes.[5,6] Zinc is widespread in biology and there is much interest in its detection In vivo where its concentration ranges from 10^{-9} mol dm^{-3} in the cytoplasm to 10^{-2} mol dm^{-3} in some vesicles.[7] Magnesium is found in the bone in macronutrient quantities, and it plays a key role in bone remodeling and skeletal development.[8] Fluorescent indicators for the determination of Mg^{2+} or Zn^{2+} are attractive targets in molecular design and synthesis. It is a challenge to design selective Zn^{2+} probes because the chemical properties of Zn^{2+} are so similar to those of Cd^{2+}. In recent years, progress in the area of chemosensors has contributed significantly to the development of a variety of Zn^{2+} probes based on quinoline, anthracene, BODIPY, and fluorescein as fluorophores.[9,10] Most of them are excellent Zn^{2+} sensors. Unfortunately, some Zn^{2+} sensors have disadvantages such as poor water-solubility or complicated synthesis methods. However, few Mg^{2+} sensors have been reported up to now.

A fluorescent probe is a molecular system for which the physicochemical properties change upon interaction with a chemical species in such a way as to produce a detectable fluorescent signal.[11] A number of signaling mechanisms have been developed and widely applied for the optical detection of different species, such as photoinduced electron/energy transfer (PET),[12] metal−ligand charge transfer (MLCT),[13] intramolecular charge transfer (ICT),[14] excimer/exciplex formation,[15] excited-state intra/intermolecular proton transfer (ESPT),[16] and C═N isomerization. Schiff bases (imines) are known to be good ligands for metal ions.[17,18] Some Schiff base−metal complexes have antitumor properties,[19] antioxidative activities,[20] and attractive electronic and photophysical properties.[21] In addition, Schiff base derivatives incorporating a fluorescent moiety are appealing tools for optical sensing of metal ions. In this paper, we synthesized three Schiff bases **1** (salicylaldehyde salicylhydrazone), **2** (salicylaldehyde benzoylhydrazone), and **3** (benzaldehyde salicylhydrazone) . They were prepared in a manner similar to that of a reported procedure (Scheme 1).[22] Imines are poorly fluorescent, in part due to isomerization of the C═N double bond in the excited state[23] and in part due to ESPT involving the phenolic protons of the salicylic amide moiety.[24] We reasonably expect that the ESPT and C═N isomerization may be inhibited upon the complexation with certain metal ions.

Received: October 28, 2010
Revised: January 18, 2011
Published: February 17, 2011

ACS Publications © 2011 American Chemical Society

Scheme 1. Synthesis of Compounds 1, 2, and 3[a]

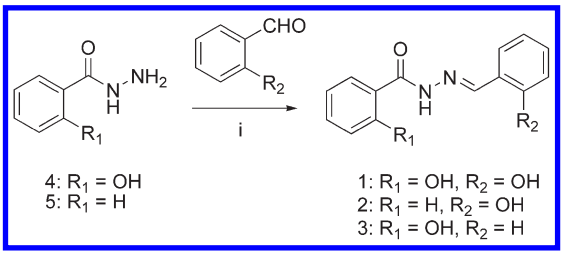

[a] Reagents and conditions: (i) ethanol, reflux, 5 h, 75%.

The spectroscopic behavior of Schiff bases shows that **1** is an excellent chemosensor for Mg^{2+} and Zn^{2+} in various organic−water mixtures. Especially, **1** can be used for Zn^{2+} monitoring in living cells. Schiff base **2** is also a good fluorescent probe for Zn^{2+} in ethanol−water.

EXPERIMENTAL SECTION

Materials. All the materials for the syntheses were purchased from commercial suppliers and used without further purification. All of the solvents used were of analytical reagent grade. Water was deionized. The solutions of the metal ions were prepared from their perchlorate salts, except for Cr^{3+} and Sn^{2+}, which were used as chloride salts, and K^+, which was available as KNO_3.

Instrumentation. The pH of the solutions was measured with a SPM-10A acidity meter (Shanghai, China). ^1H and ^{13}C NMR spectra were taken on a Varian Mercury-300 spectrometer with tetramethylsilane (TMS, 0.00 ppm) as an internal standard and DMSO-d_6 as solvent. Chemical shift multiplicities are reported as s = singlet, d = doublet, t = triplet, q = quartet, and m = multiplet. High resolution mass data (HRMS) were determined on a Bruker Daltonics APEXII 47e FT-ICR spectrometer. ESI-MS spectra were determined on a Bruker Daltonics Esquire 6000 spectrometer. Melting points were determined on a Kofler apparatus. Absorption spectra were measured on a Varian UV-Cary100 spectrophotometer using quartz cells of 1.0 cm path length. Fluorescence spectra measurements were performed on a Hitachi F-4500 spectrofluorimeter and a Shimadzu RF-540 spectrofluorophotometer equipped with quartz cuvettes of 1 cm path length with a xenon lamp as the excitation source. An excitation and emission slit of 2.5 or 5.0 nm were used for the measurements in the solid state. Quantum yields were determined by an absolute method using an integrating sphere based upon that originally developed by de Mello[25] et al. Experiments were conducted on an FLS920 from Edinburgh Instruments. The quantum yields were also determined according to the following equation: $\Phi_u = \Phi_s (F_u A_s n_u^2 / F_s A_u n_s^2)$, where Φ_u is the quantum yield, F is the integrated area under the corrected emission spectra, A is the absorbance at the excitation wavelength, n is the refractive index of the solution, and the subscripts u and s refer to the unknown and the standard, respectively. Acridine orange (λ_{ex} = 400 nm, Φ_f = 0.20) was used as the fluorescence standard.[26] All spectra were recorded at room temperature except for fluorescence microscope images. The fluorescence microscope experiment was carried out with a Nikon TE2000-5.

Synthesis of Compound ***1***. The synthesis of salicylaldehyde salicylhydrazone (**1**) was carried out as outlined in Scheme 1. The hydrazide salicylate **4** was obtained by refluxing the ester (8.5 mL, 66 mmol) and hydrazine hydrate (18 mL, 320 mmol) in absolute ethanol (20 mL) in a 100 mL one-necked bottle for 8 h (7.573 g, 75% yield). In a 200 mL three-necked bottle, compound **4** (7.573 g, 49.8 mmol) was dissolved in 30 mL of absolute ethanol. The mixture was refluxed at 80 °C until the dissolution of hydrazide salicylate. Next, 5.237 mL of salicylaldehyde (6.075 g, 49.8 mmol) was slowly dropped into the above solution. The reaction mixture was refluxed for 5 h during which an ivory white precipitate appeared. The resulting precipitate was filtered and washed three times with 15 mL of ethanol. After being dried over anhydrous sodium sulfate in vacuum, 12.111 g (95% yield) of salicylaldehyde salicylhydrazone (**1**) was obtained: mp 269 °C. ^1H NMR (300 MHz, DMSO-d_6) δ 12.01 (s, 1H), 11.76 (s, 1H), 11.18 (s, 1H), 8.66 (s, 1H), 7.87 (d, 1H, J = 7.8 Hz), 7.55 (d, 1H, J = 7.8 Hz), 7.44 (t, 1H, J = 7.8 Hz), 7.30 (t, 1H, J = 6.6 Hz), 6.89−6.98 (m, 4H) ppm. ^{13}C NMR (75 MHz, DMSO-d_6) δ 164.5, 159.0, 157.5, 149.0, 134.0, 131.7, 129.5, 128.6, 119.4, 119.1, 118.7, 117.3, 116.5, 115.6, 40.4, 40.1, 39.8, 39.5, 39.2, 39.0, 38.7 ppm. HRMS (ESI) m/z calcd for $C_{14}H_{12}N_2O_3$, 256.0848; found 257.0921 (M + 1).

Synthesis of Compound ***2***. Salicylaldehyde benzoylhydrazone (**2**) was prepared via a synthetic method analogous to that for **1** and was obtained as an ivory white solid (11.4 g, 95% yield): mp 172 °C. ^1H NMR (300 MHz, DMSO-d_6) δ 12.10 (s, 1H), 11.28 (s, 1H), 8.63 (s, 1H), 7.93 (d, 2H, J = 6.6 Hz), 7.50−7.60 (m, 4H), 7.30 (t, 1H, J = 7.8 Hz), 6.91 (t, 2H, J = 7.5 Hz) ppm. ^{13}C NMR (75 MHz, DMSO-d_6) δ 162.9, 157.5, 148.3, 132.8, 131.4, 129.6, 128.6, 127.7, 119.4, 118.7, 116.5, 40.3, 40.1, 39.8, 39.5, 39.2, 40.0, 38.7 ppm. HRMS (ESI) m/z calcd for $C_{14}H_{12}N_2O_2$, 240.0899; found 241.0972 (M + 1).

Synthesis of Compound ***3***. Benzaldehyde salicylhydrazone (**3**) was prepared via a synthetic method analogous to that for **1** and was obtained as an ivory white solid (11.4 g, 95% yield): mp 231 °C. ^1H NMR (300 MHz, DMSO-d_6) δ 11.86 (s, 2H), 8.48 (s, 1H), 7.90 (d, 1 H, J = 7.5 Hz), 7.75 (q, 2H, J = 3.2 Hz), 7.42−7.47 (m, 4H), 6.94−6.70 (m, 2H) ppm. ^{13}C NMR (75 MHz, DMSO-d_6) δ 164.8, 159.0, 148.7, 134.1, 133.8, 130.3, 128.9, 128.6, 117.2, 119.0, 117.3, 115.9, 40.3, 40.1, 39.8, 39.5, 39.2, 40.0, 38.7 ppm. HRMS (ESI) m/z calcd for $C_{14}H_{12}N_2O_2$, 240.0899; found 241.0969 (M + 1).

Synthesis of Complexes. $Zn(ClO_4)_2$ (0.1 mmol) was added to an ethanol solution containing **1** or **2** (0.1 mmol). The complexes were obtained by stirring the mixtures for 5 h. **1**−Zn^{2+}: ESI-MS m/z calcd for $C_{28}H_{22}N_4O_6Zn$, 574.1, found m/z 575.1 (M + 1). **2**−Zn^{2+}: ESI-MS m/z calcd for $C_{28}H_{22}N_4O_4Zn$, 542.2, found m/z 543.1 (M + 1).

Cell Incubation and Imaging. Human bladder cancer cell line EJ was obtained from Laboratory Center for Medical Science of Lanzhou University. Cells were cultured in RPMI 1640 (Gibco, New York, NY) supplemented with 10% fetal bovine serum (FBS, Rongye Biotech, China) and penicillin (100 U/mL)/streptomycin (100 mg/L) in an atmosphere of 5% CO_2 at 37 °C. One day before imaging, cells were seeded in 96-well flat-bottomed plates. Immediately before the experiments, cells were incubated with the probe **1** (50 μM) for 0.5 h in RPMI 1640 at 37 °C under 5% CO_2 and then washed with phosphate-buffered saline (PBS) three times before incubating with $Zn(ClO_4)_2$. Next, stained cells were incubated with 50 μM $Zn(ClO_4)_2$ for another 0.5 h, cells were rinsed with PBS three times again, and then intracelluar fluorescence imaging was performed under a Nikon Eclipse TE2000-5 inverted fluorescence microscope with a 20× objective lens (excited with blue light). The EJ cells that were only incubated with **1** (50 μM) for 0.5 h at 37 °C under 5% CO_2 were a control.

RESULT AND DISCUSSION

The electronic absorption spectra properties of **1** were investigated in *N*,*N*-dimethylformamide (DMF) or ethanol. The effects of Mg^{2+} on the absorption spectra of **1** in DMF are displayed in Figure S1 (Supporting Information). Because DMF absorbs strongly below

Scheme 2. ESPT and Distribution of the Absorption Bands to Compound 1

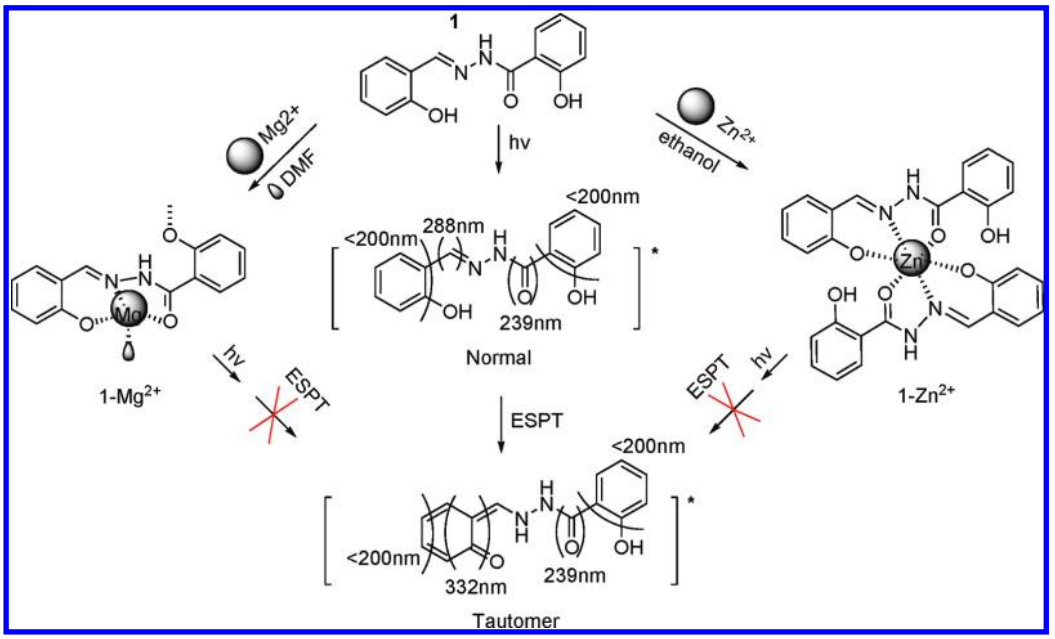

270 nm, it is difficult to observe the absorption bands of **1** at wavelengths lower than 270 nm. The absorption spectrum of **1** in ion-free solution presents two important transitions with intense absorption bands at 299 and 335 nm, respectively. As Scheme 2 describes, there is an equilibrium between the two configurations (Normal and Tautomer) due to ESPT. The band at 335 nm (332 nm in Scheme 2) is assigned to the transition of O═C−C═C−(NH) in Tautomer. The band at 299 nm (288 nm in Scheme 2) is attributed to the azomethine C═N bond, and the band at 239 nm which is assigned to C═O derived from salicyloyl hydrazone does not emerge from the DMF spectrum. After the addition of Mg^{2+}, the absorbance of compound **1** at 299 nm increases gradually; however, the peak at 335 nm starts to disappear. The spectral change indicated that the addition of Mg^{2+} ion induced the decrease of tautomer. We speculated that the nitrogen of azomethine took part in the coordination with Mg^{2+} and the formation of the **1**−Mg^{2+} complex inhibited the ESPT (Scheme 2). Moreover, two new bands appeared at 387 and 410 nm, which are certainly caused by a new, larger conjugated system (**1**−Mg^{2+} complex). We also investigated the electronic absorption spectral properties of ligands **2** (R_1 = H, R_2 = OH, Scheme 1) and **3** (R_1 = OH, R_2 = H, Scheme 1). The main difference between compounds **1**−**3** is that they have one or two OH (or H) group(s) at the 2,2′ (ortho) positions. For compounds **2** and **3**, in which one of the hydroxyl groups of compound **1** is missing, there are no new peaks centered at 400 nm after the addition of Mg^{2+} ion. We speculated that the hydroxyl groups in compound **1** (i.e., OH of the salicylic amide moiety and OH of the salicylaldimine part: R_1 = R_2 = OH in Scheme 1) were required for the selectivity for Mg^{2+}.

The absorption spectra of **1** in the absence and presence of Zn^{2+} in ethanol are depicted in Figure S2 (Supporting Information). In ion-free solution, there are three key peaks at 239 nm, 288 nm, and 332 nm, respectively. They are assigned in Scheme 2. The absorbance of compound **1** at 288 had a red shift (from 288 nm to 297 nm), and the peak at 332 nm disappeared gradually. The disappearance of the absorption band at 332 nm indicated that the formation of **1**−Zn^{2+} complex inhibited ESPT and led to the large decrease of tautomer. Because the peak at 288 nm had a red shift, we speculated that the nitrogen of azomethine was involved in the formation of the **1**−Zn^{2+} complex. In addition, the transition of C═O of salicyloyl hydrazone at 239 nm had a blue shift with slight increase in absorption. This indicates that the C═O particpates in the coordination. A new peak at 397 nm was observed with the addition of Zn^{2+}, caused by the formation of the **1**−Zn^{2+} complex. We investigated the electronic absorption spectra of **2** and **3** to determine which OH of compound **1** was involved in the coordination to Zn^{2+}. The spectra of **2** (in which the hydroxyl group of the salicylic amide moiety in compound **1** is missing) showed a change similar to that of **1** after the addition of Zn^{2+} (Figure S3, Supporting Information), which suggested that the hydroxyl group of the salicylic amide moiety (R_1 = OH) in **1** was not essential for the coordination to the Zn^{2+} ion. No change was observed in the spectra of compound **3** (R_1 = OH, R_2 = H, Scheme 1) after the injection of Zn^{2+} ions indicated the participation of R_2 = OH in the complexation of **1** with Zn^{2+} (Scheme 2). A similar coordination mode occurs between **2** and the Zn^{2+} ion.

The changes in the fluorescence emission spectra of **1** at pH ∼ 7 induced by addition of Mg^{2+} in DMF−H_2O (9:1, v/v, λ_{ex} = 410 nm) is portrayed in Figure 1. The fluorescent signal of **1** at 453 nm increases significantly with an increase in the concentration of Mg^{2+} in DMF−H_2O solution. There is a 6-fold increase of the fluorescence quantum yield Φ_f of **1** in the presence of Mg^{2+} [from 0.044 in ion-free DMF−H_2O to 0.26 at 30 μM Mg^{2+}]. In ethanol−H_2O (9:1, v/v), the maximum of the fluorescence emission band of **1** shifts from 453 nm in ion-free solution to 488 nm in the presence of Zn^{2+} and is accompanied by a 6-fold increase in Φ_f (Figure 2) [Φ_f increases from 0.05 for ion-free **1** to 0.31 in the presence of 1 equiv of Zn^{2+}]. Other ions tested, such as Li^+, Na^+, Al^{3+}, K^+, Ca^{2+}, Cr^{3+}, Mn^{2+}, Fe^{3+}, Co^{2+}, Ni^{2+}, Cu^{2+}, Ag^+, Cd^{2+}, Sn^{2+}, Ba^{2+}, Hg^{2+}, and Pb^{2+}, gave no distinct change in the spectrum of **1** in both DMF−H_2O and ethanol−H_2O. This indicated that **1** could serve as an excellent fluorescent probe for Mg^{2+} and Zn^{2+} by switching solvents. The significant increase of fluorescence can be explained as follows: Imine **1** is poorly fluorescent in part due to isomerization of the C═N double bond in the excited state and in part due to excited-state proton transfer (ESPT) involving the phenolic protons

dx.doi.org/10.1021/jp110305k |J. Phys. Chem. A 2011, 115, 1609–1616

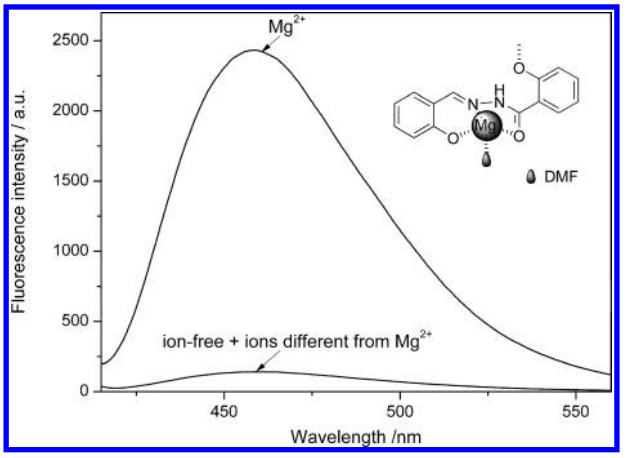

Figure 1. Fluorescence emission spectra of **1** (30 μM) in the absence (ion-free) and presence of 1 equiv of various metal ions in DMF−H_2O (9:1, v/v) solution. λ_{ex} = 410 nm.

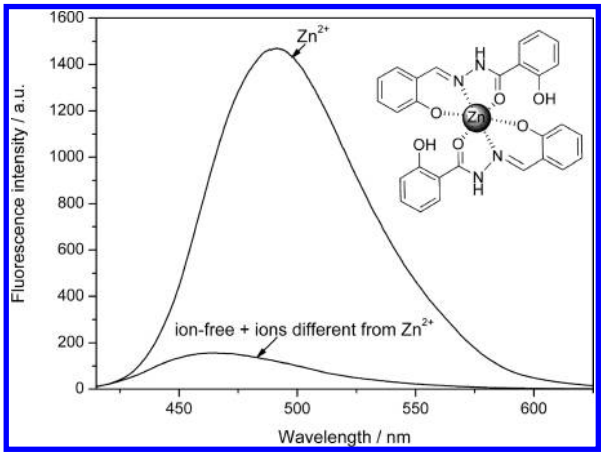

Figure 2. Fluorescence emission spectra of **1** (30 μM) in the absence (ion-free) and presence of 1 equiv of various metal ions in ethanol−H_2O (9:1, v/v) solution, λ_{ex} = 390 nm.

of the salicylic amide moiety. Upon stable chelation with cartain metal ions, the C═N isomerization is inhibited (Scheme 3); additionally, the coordination of **1** with the metal ion prevents ESPT (Scheme 2), leading to fluorescence enhancement. Moreover, the reaction of a metal ion with a chelating agent induces rigidity in the resulting molecule and tends to produce a large CHEF effect which induces the large enhancement of fluorescence.

We also investigated the effect of Zn^{2+} and Mg^{2+} on the fluorescence properties of compounds **2** and **3**. Compound **3** exhibited no spectral change from any metal ion in any of the solvents tested (methanol, ethanol, acetone, acetonitrile, chloroform, DMF, and DMSO). Mg^{2+} did not induce any spectral change of **2** in the above solvents. However, **2** is a good indicator for Zn^{2+} in ethanol−H_2O (9:1, v/v). The change of fluorescence emission spectra of **2** after the addition of Zn^{2+} ions is shown in Figure 3. In the absence of Zn^{2+}, the fluorescence emission peak of **2** was very weak due to isomerization of the C═N double bond and ESPT effect. Upon addition of Zn^{2+} to the solution of **2**, there was a significant enhancement in the fluorescence emission band with a red shift, reaching a maximum at 495 nm. This enhancement of fluorescence intensity was due to inhibition of the C═N isomerization and ESPT effect after the injection of Zn^{2+} into the solution mixture of **2**.

Scheme 3. C═N Isomerization

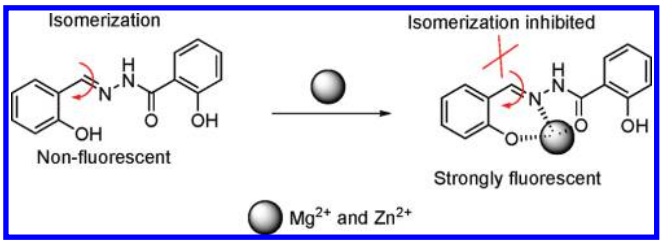

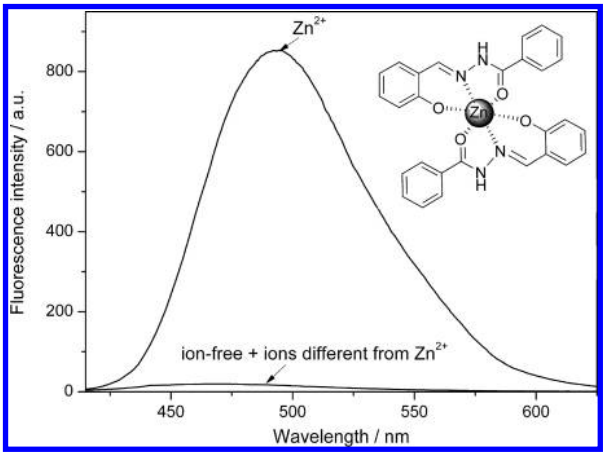

Figure 3. Fluorescence emission spectra of **2** (30 μM) in the absence (ion-free) and presence of 1 equiv of different metal ions in ethanol−H_2O (9:1, v/v) solution. λ_{ex} = 390 nm.

Moreover, with coordination to the metal ion, an extended π-electroconjugation system was formed. At the same time, a selective chelation-enhanced fluorescence (CHEF) effect was observed, which was a significant enhancement in the fluorescence intensity of Schiff base **2**. No change in the fluorescence spectra could be found after the addition of other ions to the solution of **2**. This interesting feature reveals that **2** can serve as an excellent selective fluorescent chemosensor for Zn^{2+}. The fluorescence spectra of **1**, **2**, and **3** indicated that the CONHN═CH function, which is present in all three compounds (**1**−**3**), is not sufficient to warrant selectivity for a specific metal ion. Indeed, the *o*-hydroxy groups play decisive roles in the selectivity. For the complex between **1** and Mg^{2+} in DMF−H_2O solution, the two hydroxyl groups (i.e., OH of the salicylic amide moiety and OH of the salicylaldimine part: R_1 = R_2 = OH in Scheme 1) are needed for coordination of **1** to Mg^{2+}. The selectivity of **1** and **2** for Zn^{2+} requires the OH of the salicylaldimine moiety, indicating the participation of R_2 = OH in the complexation of Zn^{2+}. However, the hydroxyl group of the salicylic amide moiety is not necessary for the coordination of Zn^{2+} to ligand.

The fluorescence titration experiments were performed by mixing various amounts of metal ions with **1**. Figures 4 and 5 show the fluorescence emission changes of **1** after the addition of various concentrations of Mg^{2+} and Zn^{2+}, respectively, in 9:1 (v/v) organic/aqueous solvent. For **1**−Mg^{2+}, the fluorescence intensity enhanced gradually along with the changes in concentration of Mg^{2+} ions. It did not reach a maximum until the concentration of ions achieved 1 equiv. For **1**−Zn^{2+}, the fluorescence intensity increased obviously until the concentration of Zn^{2+} achieved 0.5 equiv. The ground-state dissociation constants K_d of the **1**−Mg^{2+} and **1**−Zn^{2+} complexes were determined by direct fluorimetric titration as a function of

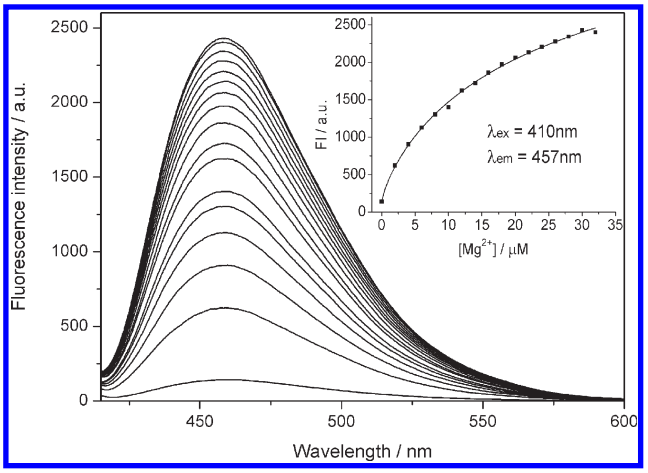

Figure 4. Fluorescence spectra of **1** (30 μM) in the absence and presence of $Mg(ClO_4)_2$ (0−30 μM) in 10% aqueous DMF. λ_{ex} = 410 nm.

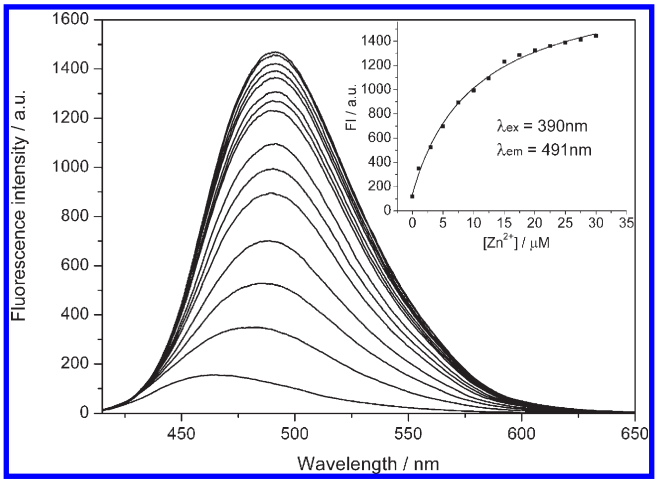

Figure 5. Fluorescence spectra of **1** (30 μM) in the absence and presence of $Zn(ClO_4)_2$ (0−15 μM) in 10% aqueous ethanol . λ_{ex} = 390 nm.

$[M^{2+}]$ (M^{2+} − Mg^{2+} or Zn^{2+}). Nonlinear curve fitting of eq 1[27]

$$F = \frac{F_{max}[M]^n + F_{min}K_d}{K_d + [M]^n} \quad (1)$$

to the fluorescence data F recorded as a function of $[M^{2+}]$ yields values of K_d, the fluorescence signals F_{min} and F_{max} at minimal and maximal $[M^{2+}]$, respectively (corresponding to the free and M^{2+} bound forms of the probe, respectively), and n (the number of M^{2+} bound per probe). The ground-state dissociation constants K_d of the **1**−Mg^{2+} complex was found to be 33.84 ± 3.19 μM (Figure 4 inset). Fitting eq 1 to the steady-state fluorescence data F with n, K_d, F_{min}, and F_{max} as freely adjustable parameters always gave values of n close to 1; n was kept fixed at 1 in the final curve fittings, which indicated that **1** formed a 1:1 complex with Mg^{2+}. This binding mode was also supported by the data of Job's plots evaluated from the fluorescence spectra of **1** and Mg^{2+} with a total concentration of 100 μM (Figure S4, Supporting Information).[28] The ground-state dissociation constants K_d of the **1**−Zn^{2+} complex were found to be 35.87 ± 3.59 μM. Job's plots (Figure S5, Supporting Information) and fitting eq 1 to the steady-state fluorescence data F (Figure 5 inset) gave values of n close to 0.5, which indicated a 2:1 stoichiometry between **1** and Zn^{2+}.

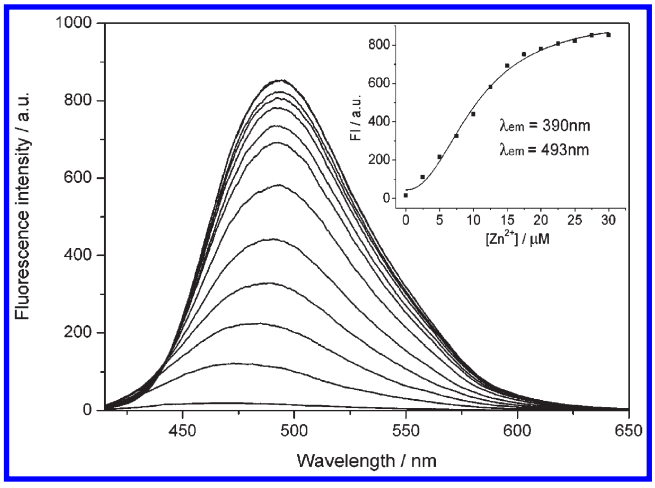

Figure 6. Fluorescence spectra of **2** (30 μM) in the absence and presence of $Zn(ClO_4)_2$ (0−15 μM) in 10% aqueous ethanol. λ_{ex} = 390 nm.

Nonlinear curve fitting of eq 1 to the fluorescence data F recorded as a function of $[Zn^{2+}]$ yields ground-state dissociation constants K_d and n of the **2**−Zn^{2+} complex as 42.38 ± 3.20 μM and 0.5 (Figure 6 inset), respectively. Job's plots confirm the value of n (Figure S6, Supporting Information), which indicates that the coordination mode of probe **2** with Zn^{2+} is also 2:1 stoichiometry.

Job's plots suggested that a 1:1 stoichiometry is the most likely binding mode between **1** and Mg^{2+}. The dominating peak in ESI mass spectra of **1**−Mg^{2+} (Figure S16, Supporting Information) was in agreement on a 1:1 stoichiometry. The peak at m/z = 352.1 (calcd =352.1) corresponding to $[Mg\mathbf{L^1}(DMF)]^+$ ($\mathbf{L^1}$ = **1**) was observed. Thus, according to the above spectral data and some structures of Mg^{2+} complexes,[29] we presented the probable binding mode between **1** and Mg^{2+} as shown in Figure 1 inset. DMF molecules were involved in the coordination of Schiff base **1** to Mg^{2+}, and some hydrogen bonding with the remaining OH group in Schiff base **1**. Maybe there was another bonding mode: Each Mg^{2+} center is coordinated to a chelating ligand **1** and the OH of a neighboring [**1**−Mg^{2+}] unit. Note that the peaks at m/z = 269.0 (calcd = 269.0) and m/z = 279.1 (calcd =279.1) were attributed to $[Mg(DMF)_2(ClO_4)]^+$ and $[Mg\mathbf{L^1} + H]^+$ ($\mathbf{L^1}$ = **1**), respectively. Perhaps the coordination modes between **1** and Mg were diversified. As demonstrated for complexes **1**−Zn^{2+} and **2**−Zn^{2+}, **1** and **2** can serve as good fluorescent probes for Zn^{2+} ion; however, **3** has no selectivity for Zn^{2+}. On the basis of the structures of **1**, **2**, and **3**, we estimated the configuration of the **1**−Zn^{2+} complex as displayed in Figure 2 inset. More direct evidence of this binding mode was obtained from the ESI mass spectra of **1**−Zn^{2+} (Figure S17, Supporting Information). A peak at m/z = 575.2 (calcd =575.1) corresponding to $[Zn(\mathbf{L^1})_2 + H]^+$ ($\mathbf{L^1}$ = **1**) was observed. This binding mode was also supported by Job's plots. Job's plots also indicated a 2:1 stoichiometry between **2** and Zn^{2+}. The complex **2**−Zn^{2+} exhibited peak at m/z = 543.2 (calcd =543.1), which corresponds to $[Zn(\mathbf{L^2})_2 + H]^+$ (Figure S18, Supporting Information, $\mathbf{L^2}$ = **2**). Figure 3 inset shows the proposed structure of the **2**−Zn^{2+} complex. However, other metal ions fail to form such a rigid framework, probably because of several combined influences cooperating to achieve the unique selectivity for the Mg^{2+} and Zn^{2+} ion, such as the suitable coordination geometry conformation of the bischelating Schiff base receptor, the appropriate ion radius and sufficient binding energy of the Mg^{2+} and Zn^{2+}, and the suitable coordination ability of the specific solvent.

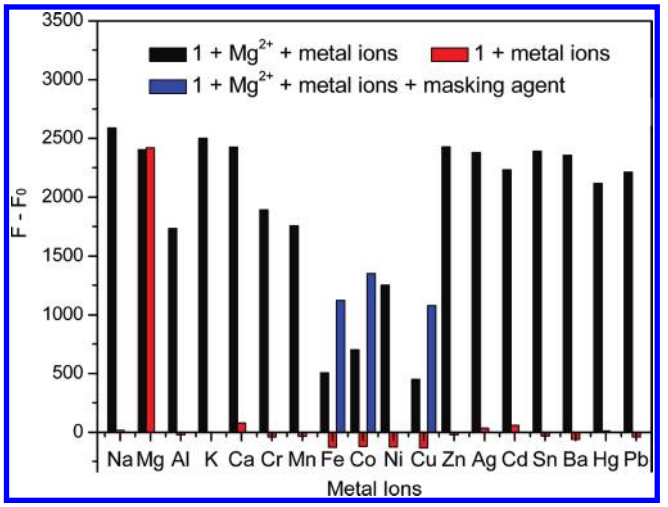

Figure 7. Metal-ion response for **1** (30 μM) in the absence (F_0) and presence (F) of metal ions in DMF−water (9/1, v/v). One equivalent of NaF was used for masking Fe^{3+}, and 1 equiv of $Na_2S_2O_3$ was used for masking Cu^{2+} and Co^{2+}.

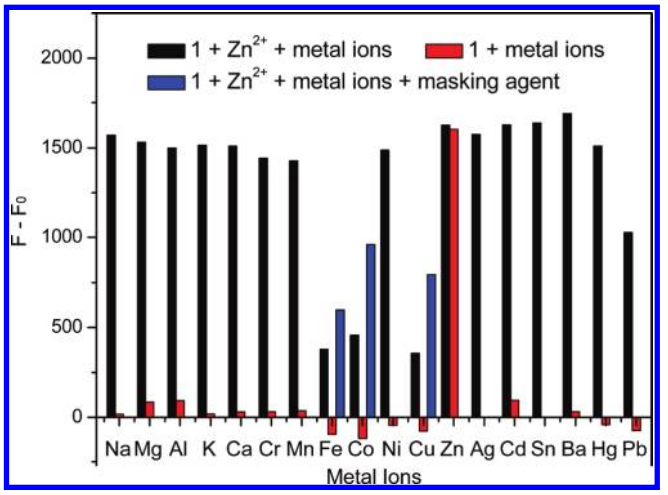

Figure 8. Metal-ion response for **1** (30 μM) in the absence (F_0) and presence (F) of metal ions in ethanol−water (9/1, v/v). One equivalent of NaF was used for masking Fe^{3+}, and 1 equiv of $Na_2S_2O_3$ was used for masking Cu^{2+} and Co^{2+}.

It is known that achieving a high selectivity for the analyte of interest over a complex background of potentially competing species is a challenging task in sensor development. Figure 7 and Figure 8 illustrate the fluorescence response of **1** to Mg^{2+} and Zn^{2+} in the presence of other metal ions, respectively. Except for Fe^{3+}, Co^{2+}, and Cu^{2+}, a background of most competing metal ions does not interfere with the detection by **1** of Mg^{2+} in DMF−H_2O and of Zn^{2+} in ethanol−H_2O. However, the addition of 1 equiv of masking agent NaF to the solution of **1** containing Fe^{3+} and Mg^{2+} in DMF−H_2O or Fe^{3+} and Zn^{2+} in ethanol−H_2O weakens the influence of Fe^{3+}.[30] Analogously, $Na_2S_2O_3$ was used to weaken the interference of Cu^{2+} and Co^{2+}.

Next, we investigated whether the selectivity of **1** for metal ions could be produced in other solvents (Figure S7, Supporting Information). The addition of Mg^{2+} to **1** in other solvents, such as methanol, ethanol, acetonitrile, acetone, chloroform, and dimethyl sulfoxide (DMSO), induced negligible fluorescence enhancement.

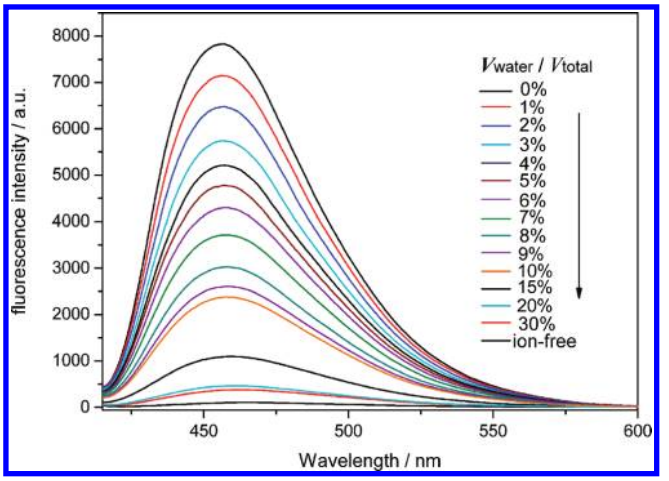

Figure 9. Fluorescence emission spectra of **1** (30 μM) in various mixing ratios of DMF−water solution (%, v/v). λ_{ex} = 410 nm.

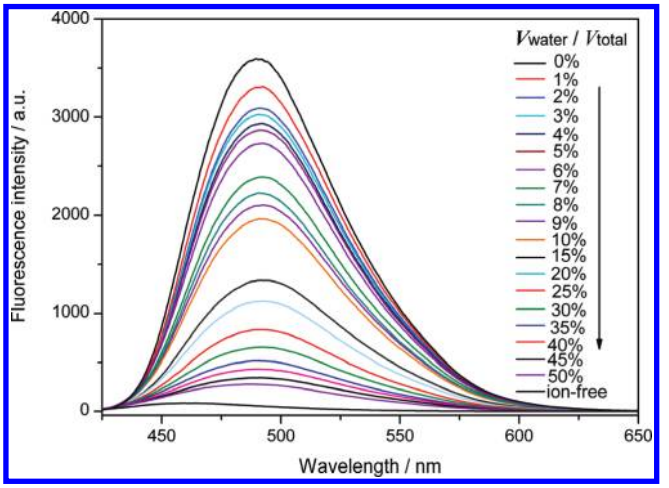

Figure 10. Fluorescence emission spectra of **1** (30 μM) in various mixing ratios of ethanol−water solution (%, v/v). λ_{ex} = 390 nm.

Except for ethanol, methanol, and acetone, the change of the fluorescence spectra after Zn^{2+} was added to **1** was not significant enough to be worth considering in other solvents. Zn^{2+} changed the spectrum of **1** in methanol and acetone; however, the enhancement of fluorescence intensity of **1** upon the addition of Zn^{2+} in methanol and acetone was less than that in ethanol. The selectivity of **1** for Zn^{2+} in ethanol is better than that in any other solvent. In addition, the fluorescence intensity changed as a function of the ratio of organic solvent to water. The fluorescence intensity is quenched gradually by increasing the amount of water.

The fluorescence change that occurred upon addition of water to a DMF solution containing **1** and Mg^{2+} ion was investigated. The fluorescence intensity of a solution containing **1** and Mg^{2+} ion declined gradually with the increase in the concentration of water (Figure 9). In water-free DMF solution containing **1** and Mg^{2+}, there is obvious blue fluorescence. The fluorescence became very weak when the content of water reached 30% in solution (keeping the concentration of **1** and Mg^{2+} constant). Figure 10 shows the change in emission spectra of ethanol solution containing **1** and Zn^{2+} with the increase of water. A similar change occurred in the fluorescence spectra of the **2**−Zn^{2+} complex in ethanol (Figure S8, Supporting Information).

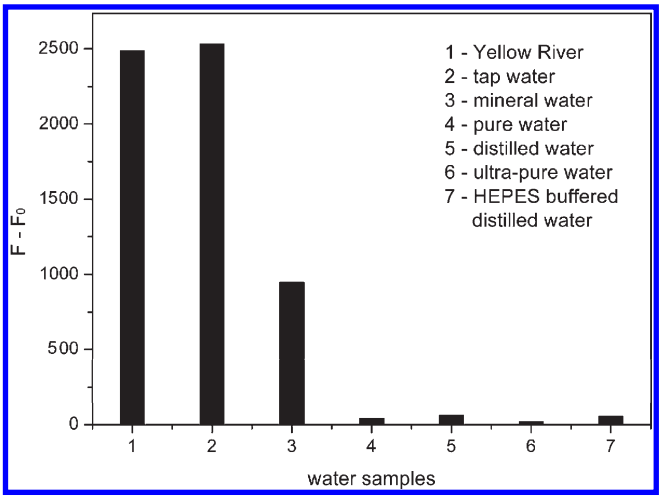

Figure 11. Fluorescence intensity of DMF solution of **1** (30 μM) with addition of various 10% (%, v/v) water samples.

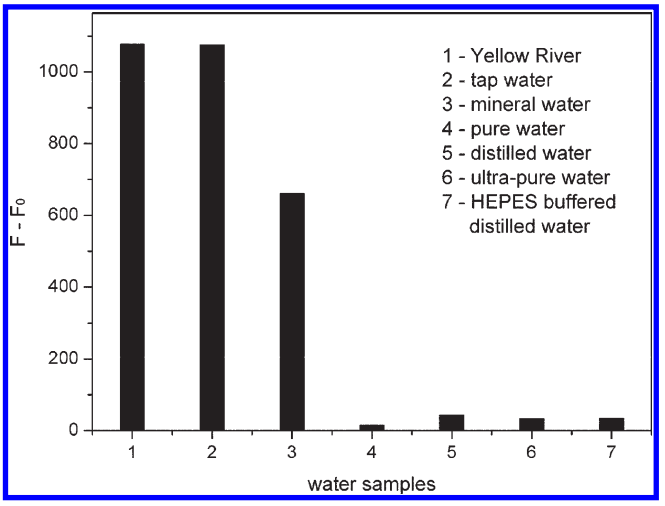

Figure 12. Fluorescence intensity of ethanol solution of **1** (30 μM) with addition of various 10% (%, v/v) water samples.

Generally, one of the most important and useful applications for a fluorescent probe is the detection of metal ions in water samples. Herein, we choose several water samples from different water sources: water from Yellow River, tap water, mineral water, pure water, distilled water, ultrapure water, and HEPES-buffered distilled water. Probe **1** is sensitive enough to detect the concentrations of Mg^{2+} in these water samples. The change of fluorescence intensity after the addition of 10% water to the DMF solution of **1** is shown in Figure 11. The fluorescence intensity of **1** upon the addition of 10% Yellow River and tap water increased significantly, which indicates that the content of Mg^{2+} in both water samples is high. Figure 11 also shows the concentration of Mg^{2+} ion in mineral water is medium, and in other water samples is lower. Figure 12 displays the change of flurescence intensity after the addition of 10% water to the ethanol solution of **1**. The enhancement of fluorescence with the addition of Yellow River and tap water indicates the existence of Zn^{2+} ions in these water samples. Figure 12 shows that the concentration of Zn^{2+} ions in mineral water is lower than that in Yellow River and tap water, which suggests that the amount of Zn^{2+} ion in other samples is very small. The change of fluorescence intensity after the addition of 10% water to the ethanol solution of **2** is shown in Figure S9 (Supporting Information).

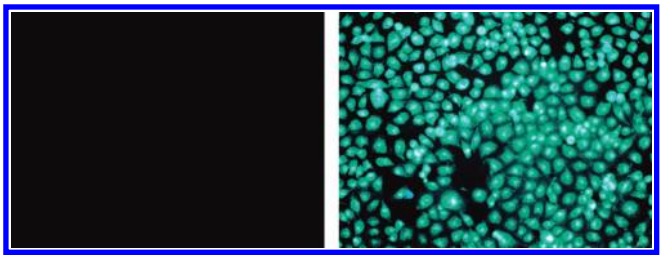

Figure 13. Fluorescence microscope images of human bladder cancer cell line EJ. EJ cells loaded with probe **1** (50 μM) for 30 min under a 20× objective lens (left). Fluorescence image of **1**-stained EJ cells exposed to 50 μM Zn^{2+} for 30 min under a 20× objective lens (right). Incubation was performed at 37 °C.

Subsequent experiments probed the ability of **1** to track Zn^{2+} levels in living cells using fluorescence microscopy. To determine the cell permeability of **1**, human bladder cancer cell line EJ was incubated with **1**. EJ cells incubated with 50 μM **1** for up to 30 min at 37 °C show negligible intracellular fluorescence. In contrast, **1**-stained cells exposed to 50 μM Zn^{2+} for 30 min at 37 °C display enhanced cytosolic fluorescence (Figure 13). Further control experiments without ligand **1** or Zn^{2+} give no fluorescence over background levels. Taken together, it clearly demonstrated that the probe is membrane-permeable, and the fluorescence change in the human bladder cancer cell line EJ was really due to the synchronous appearance of **1** and Zn^{2+}. The result confirmed that the probe **1** can be used to image intracellular Zn^{2+} in living cells. It should therefore be potentially useful to study the content or bioactivity of Zn^{2+} in living cells.

CONCLUSIONS

In conclusion, we synthesized two Schiff base fluorescent indicators **1** and **2**. **1** is an excellent indicator with solvent-dependent, ion-tunable selectivity for Mg^{2+} and Zn^{2+}. The presence of *o*-hydroxy groups and the nature of the solvent play crucial roles in the selectivity for metal ions and the switch of selectivity from Mg^{2+} to Zn^{2+}. In addition, **1** is membrane-permeable and can also be used for Zn^{2+} monitoring in living cells. Schiff base **2** has selectivity to Zn^{2+} ion in various solvents. Many other ions tested, such as Li^{+}, Na^{+}, Al^{3+}, K^{+}, Ca^{2+}, Cr^{3+}, Mn^{2+}, Fe^{3+}, Co^{2+}, Ni^{2+}, Cu^{2+}, Ag^{+}, Cd^{2+}, Sn^{2+}, Ba^{2+}, Hg^{2+}, and Pb^{2+}, have no influence on the spectrum of **1** or **2**. The luminescence mechanism is as follows: The formation of a rigid framework between Schiff bases and Mg^{2+} or Zn^{2+} inhibits the C=N isomerization and ESPT, leading to fluorescence enhancement. Simultaneously, the chelation between metal ion and ligand causes a large CHEF effect, which induces the increase of fluorescence intensity.

ASSOCIATED CONTENT

Supporting Information. ^{1}H NMR spectrum, ^{13}C NMR spectrum, and MS spectra for the compounds and selected spectroscopic data. This material is available free of charge via the Internet at http://pubs.acs.org.

AUTHOR INFORMATION

Corresponding Author

*Tel: +86-0931-8915151. Fax: +86-0931-8912582. E-mail: liuws@lzu.edu.cn.

■ ACKNOWLEDGMENT

This study was supported by the NSFC (Grant Nos. 20771048, 20931003) and the Fundamental Research Funds for the Central Universities (lzujbky-2009-k06).

■ REFERENCES

(1) Haugland, R. P. *Handbook of Fluorescent Probes and Research Products*, 9th ed.; Molecular Probes: Eugene, OR, 2002; Chapter 20.

(2) (a) Desvergne, J. P.; Czarnik, A. W. *Chemosensors of Ion and Molecule Recognition*; Kluwer: Dordrecht, 1997. (b) Valeur, B. *Molecular Fluorescence. Principles and Applications*; Wiley-VCH: Weinheim, Germany, 2002.

(3) (a) Amendola, V.; Fabbrizzi, L.; Forti, F.; Licchelli, M.; Mangano, C.; Pallavicini, P.; Poggi, A.; Sacchi, D.; Taglieti, A. *Coord. Chem. Rev.* **2006**, *250*, 273–299. (b) Rurack, K.; Resch-Genger, U. *Chem. Soc. Rev.* **2002**, *31*, 116–127. (c) Valeur, B.; Leray, I. *Coord. Chem. Rev.* **2000**, *205*, 3–40.

(4) (a) Beavis, A. D.; Powers, M. F. *J. Biol. Chem.* **1989**, *264*, 17148–17155. (b) Bray, T. M.; Bettger, W. *J. Biol. Med.* **1990**, *8*, 281–291.

(5) Anast, C. S.; Mohs, J. M.; Kaplan, S. L.; Burns, T. W. *Science* **1972**, *177*, 606–608.

(6) Stefanidou, M.; Maravelias, C.; Dona, A.; Spiliopoulou, C. *Arch. Toxicol.* **2006**, *80*, 1–9.

(7) (a) Williams, R. J. P. *Polyhedron* **1987**, *6*, 61–69. (b) Cunane, S. C. *Zinc: Clinical and Biochemical Significance*; CRC Press: Boca Raton, 1988. (c) Vallee, B. L.; Auld, D. S. *Proc. Natl. Acad. Sci. U.S.A.* **1990**, *87*, 220–224. (d) Fausto de Silva, J. J.; Williams, R. J. P. *Biological Chemistry of the Elements*; Oxford University Press: NewYork, 1991. (e) Vallee, B. L.; Auld, D. S. *Acc. Chem. Res.* **1993**, *26*, 543–551. (f) Kaim, K.; Schwederski, B. *Bioinorganic Chemistry: Inorganic Elements in the Chemistry of Life*; Wiley: Chichester, 1994.

(8) (a) Bogoroch, R.; Belanger, L. F. *Anat. Rec.* **1975**, *183*, 437–447. (b) Trowbridge, H. O.; Seltzer, J. L. *J. Periodontal Res.* **1967**, *2*, 147–153.

(9) (a) Pearce, D. A.; Jotterand, N.; Carrico, I. S.; Imperiali, B. *J. Am. Chem. Soc.* **2001**, *123*, 5160–5161. (b) Zhang, Y.; Guo, X. F.; Si, W. X.; Jia, L. H.; Qian, X. H. *Org. Lett.* **2008**, *10*, 473–476.

(10) (a) Ajayaghosh, A.; Carol, P.; Sreejith, S. *J. Am. Chem. Soc.* **2005**, *127*, 14962–14963. (b) Akkaya, E. U.; Huston, M. E.; Czarnik, A. W. *J. Am. Chem. Soc.* **1990**, *112*, 3590–3593. (c) Gong, H.; Zheng, Q.; Zhang, X.; Wang, D.; Wang, M. *Org. Lett.* **2006**, *8*, 4895–4898. (d) Burdette, S. C.; Frederickson, C. J.; Bu, W.; Lippard, S. J. *J. Am. Chem. Soc.* **2003**, *125*, 1778–1787. (e) Wu, Y.; Peng, X.; Guo, B.; Fan, J.; Zhang, Z.; Wang, J.; Cui, A.; Gao, Y. *Org. Biomol. Chem.* **2005**, *3*, 1387–1392.

(11) (a) Valeur, B. *Molecular Fluorescence Principles and Applications*; Wiley-VCH Verlag GmbH: New York, 2001; pp 341−348. (b) Vance, D. H.; Czarnik, A. W. *J. Am. Chem. Soc.* **1994**, *116*, 9397–9398. (c) Kim, S. K.; Yoon, J. *Chem. Commun.* **2002**, 770–771.

(12) Gunnlaugsson, T.; Davis, A. P.; O'Brien, J. E.; Glynn, M. *Org. Lett.* **2002**, *4*, 2449–2452.

(13) (a) Beer, P. D. *Acc. Chem. Res.* **1998**, *31*, 71–80. (b) Kim, M. J.; Konduri, R.; Ye, H.; MacDonnell, F. M.; Puntoriero, F.; Serroni, S.; Campagna, S.; Holder, T.; Kinsel, G.; Rajeshwar, K. *Inorg. Chem.* **2002**, *41*, 2471–2476.

(14) (a) Xu, Z.; Xiao, Y.; Qian, X.; Cui, J.; Cui, D. *Org. Lett.* **2005**, *7*, 889–892. (b) Wu, F. Y.; Jiang, Y. B. *Chem. Phys. Lett.* **2002**, *355*, 438–444. (c) Wang, J. B.; Qian, X. H.; Cui, J. N. *J. Org. Chem.* **2006**, *71*, 4308–4311.

(15) (a) Nishizawa, S.; Kato, Y.; Teramae, N. *J. Am. Chem. Soc.* **1999**, *121*, 9463–9464. (b) Yuasa, H.; Miyagawa, N.; Izumi, T.; Nakatani, M.; Izumi, M.; Hashimoto, H. *Org. Lett.* **2004**, *6*, 1489–1492. (c) Schazmann, B.; Alhashimy, N.; Diamond, D. *J. Am. Chem. Soc.* **2006**, *128*, 8607–8614. (d) Chandrasekharan, N.; Kelly, L. A. *J. Am. Chem. Soc.* **2001**, *123*, 9898–9899. (e) Wu, J. S.; Zhou, J. H.; Wang, P. F.; Zhang, X. H.; Wu, S. K. *Org. Lett.* **2005**, *7*, 2133–2136.

(16) Zhang, X.; Guo, L.; Wu, F. Y.; Jiang, Y. B. *Org. Lett.* **2003**, *5*, 2667–2670.

(17) Salmon, L.; Thuéry, P.; Rivière, E.; Ephritikhine, M. *Inorg. Chem.* **2006**, *45*, 83–93.

(18) Epstein, D. M.; Choudhary, S.; Churchill, M. R.; Keil, K. M.; Eliseev, A. V.; Morrow, J. R. *Inorg. Chem.* **2001**, *40*, 1591–1596.

(19) da Silveira, V. C.; Luz, J. S.; Oliveira, C. C.; Graziani, I.; Ciriolo, M. R.; Ferreira, A. M. D. C. *J. Inorg. Biochem* **2008**, *102*, 1090–1103.

(20) (a) Padhye, S.; Kauffman, G. B. *Coord. Chem. Rev.* **1985**, *63*, 127–160. (b) Li, Y.; Yang, Z. Y. *Inorg. Chim. Acta* **2009**, *362*, 4823–4831.

(21) Kasselouri, S.; Garoufis, A.; Katehanakis, A.; Kalkanis, G.; Perlepes, S. P.; Hadjiliadis, N. *Inorg. Chim. Acta* **1993**, *207*, 255–258. (b) Padhye, S.; Kauffman, G. B. *Coord. Chem. Rev.* **1985**, *63*, 127–160.

(22) Sacconi, L. *Z. Anorg. Chem.* **1954**, *275*, 249–256.

(23) Wu, J.; Liu, W.; Zhuang, X.; Wang, F.; Wang, P.; Tao, S.; Zhang, X.; Wu, S.; Lee, S. T. *Org. Lett.* **2007**, *9*, 33–36.

(24) Royzen, M.; Durandin, A.; Young, V. G.; Geacintov, N. E.; Canary, J. W. *J. Am. Chem. Soc.* **2006**, *128*, 3854–3855.

(25) de Mello, J. C.; Wittmann, H. F.; Friend, R. H. *Adv. Mater.* **1997**, *9*, 230–&.

(26) Du, H.; Fuh, R. A.; Li, J.; Corkan, A.; Lindsey, J. S. *Photochem. Photobiol.* **1998**, *68*, 141–142.

(27) Cielen, E.; Stobiecka, A.; Tahri, A.; Hoornaert, G. J.; De Schryver, F. C.; Gallay, J.; Vincent, M.; Boens, N. *J. Chem. Soc., Perkin Trans. 2* **2002**, 1197–1206.

(28) Vosburgh, W. C.; Cooper, G. R. *J. Am. Chem. Soc.* **1941**, *63*, 437–442.

(29) (a) Byrn, M. P.; Curtis, C. J.; Hsiou, Y.; Khan, S. I.; Sawin, P. A.; Tendick, S. K.; Terzis, A.; Strouse, C. E. *J. Am. Chem. Soc.* **1993**, *115*, 9480–9497. (b) Wagner, C. C.; Baran, E. J.; Piro, O. E. *J. Inorg. Biochem.* **1999**, *73*, 259–263.

(30) Evtugyn, G. A.; Stoikov, I. I.; Beljyakova, S. V.; Shamagsumova, R. V.; Stoikova, E. E.; Zhukov, A. Y.; Antipin, I. S.; Budnikov, H. C. *Talanta* **2007**, *71*, 1720–1727.